Structure, Vol. 10, 557–567, April, 2002, ©2002 Elsevier Science Ltd. All rights reserved. PII S0969-2126(02)00740-2

Crystal Structures of S100A6 in the Ca^{2+}-Free and Ca^{2+}-Bound States: The Calcium Sensor Mechanism of S100 Proteins Revealed at Atomic Resolution

Ludovic R. Otterbein, Jolanta Kordowska, Carlos Witte-Hoffmann, C.-L. Albert Wang, and Roberto Dominguez[1]
Boston Biomedical Research Institute
64 Grove Street
Watertown, Massachusetts 02472

Summary

S100A6 is a member of the S100 family of Ca^{2+} binding proteins, which have come to play an important role in the diagnosis of cancer due to their overexpression in various tumor cells. We have determined the crystal structures of human S100A6 in the Ca^{2+}-free and Ca^{2+}-bound states to resolutions of 1.15 Å and 1.44 Å, respectively. Ca^{2+} binding is responsible for a dramatic change in the global shape and charge distribution of the S100A6 dimer, leading to the exposure of two symmetrically positioned target binding sites. The results are consistent with S100A6, and most likely other S100 proteins, functioning as Ca^{2+} sensors in a way analogous to the prototypical sensors calmodulin and troponin C. The structures have important implications for our understanding of target binding and cooperativity of Ca^{2+} binding in the S100 family.

Introduction

In higher eukaryotes, an extensive repertoire of Ca^{2+} binding proteins translate transient increases in intracellular Ca^{2+} levels into a multitude of cellular processes [1]. The vast majority of these proteins bind Ca^{2+} through helix-loop-helix structures that usually exist in pairs and are referred to as EF-hand motifs [2, 3]. While several EF-hand proteins, including calmodulin and troponin C, work as Ca^{2+} sensors, undergoing structural changes that expose target binding sites upon Ca^{2+} binding, others, such as calbindin D_{9k}, exhibit little structural change and are thought to work as Ca^{2+} buffers [4].

Most S100 proteins form dimers in solution. Each subunit is a 10–12 kDa acidic molecule with two EF-hand Ca^{2+} binding domains. While the C-terminal EF-hand displays a canonical 12 amino acid, parvalbumin-like Ca^{2+} binding loop, the N-terminal EF-hand, which is usually referred to as the S100-hand, encompasses 14 amino acids and has a lower affinity for Ca^{2+} [5, 6]. Observed deviations from this common description are the facts that (1) some S100 proteins have lost their ability to bind either one or both of the Ca^{2+} ions while still adopting a Ca^{2+}-bound-like conformation [7–9]; (2) there is at least one monomeric member in the family, calbindin D_{9k} [10]; and (3) some S100 proteins form heterodimers [5].

In contrast to calmodulin, which is ubiquitously expressed, S100 proteins are expressed in a cell-specific manner. Most S100 genes appear clustered within human chromosome 1q21 [11], a region that is often altered in transformed cells, consistent with a role in tumor progression [6]. The expression of the S100A6 gene, in particular, is increased in leukemia cells [12] and during the G1 phase of the cell cycle [13], implying a role in cell cycle progression (thus, S100A6 is also known as calcyclin). Experiments at the protein level show that S100A6 is overexpressed in numerous human cancer cells [14–16]. It has also been reported that S100A6 may be involved in reversing the inhibition exerted by caldesmon on smooth muscle contraction [17]. Binding of S100A6 to the regulatory domain of annexin XI, a Ca^{2+}-dependent phospholipid binding protein, has been connected with a potential role in cell proliferation and differentiation [18].

Three-dimensional structures of S100 proteins in the Ca^{2+}-bound form have been determined by X-ray crystallography [7, 19–22] and NMR spectroscopy [23–25]. Recently, three structures of S100 proteins bound to target peptides have been also reported: S100A10-annexin II [8], S100A11-annexin I [9], and S100B-p53 regulatory peptide [26]. Contrary to what might be expected, the binding site and orientation for the two annexin peptides is different from that of the p53 peptide. Thus, interpretation of the current structural data would suggest that target binding by different S100 proteins involves different sites.

Three NMR structures of S100 proteins, corresponding to the Ca^{2+}-free (or apo) state, are also available [27–29]. However, there is disagreement concerning these Ca^{2+}-free structures [24, 30, 31]. For example, the structures of Ca^{2+}-free and Ca^{2+}-bound rabbit S100A6 are very similar, leading the authors to question the role of S100 proteins as Ca^{2+} sensors [23, 29]. In contrast, the structures of Ca^{2+}-free and Ca^{2+}-bound rat S100B, which is similar in sequence to S100A6, reveal a major conformational change of helix III upon Ca^{2+} binding [24, 28]. A higher resolution update of the structure of Ca^{2+}-free rabbit S100A6 appears to confirm the existence of significant differences between the structures of S100A6 and S100B [31]. Groves et al. [30] have suggested that these discrepancies might arise from modeling errors due to insufficient structural constraints.

We describe here the X-ray crystal structures of *E. coli*-expressed human S100A6 in the Ca^{2+}-free and Ca^{2+}-bound states to resolutions of 1.15 Å and 1.44 Å, respectively. In both states, S100A6 forms dimers stabilized by hydrophobic interactions between helices I and IV of each monomer. Ca^{2+} binding is responsible for an $\sim$86° reorientation of helix III and marked changes in the positioning and structure of helix II, the linker loop between helices II and III, and the C-terminal end of helix IV. The combination of these structural differences results in a dramatic change in the global shape and charge distribution of the S100A6 dimer, leading to the

[1]Correspondence: dominguez@bbri.org

Key words: S100A6; calcyclin; Ca^{2+} binding; Ca^{2+} sensor; X-ray; Ca^{2+}-free structure; Ca^{2+}-bound structure

exposure of two symmetrically positioned target binding sites. These findings are consistent with the notion that S100A6 and probably other S100 proteins function as Ca^{2+} sensors. Also discussed here are the potential implications of these findings for our understanding of target binding and cooperativity of Ca^{2+} binding in the S100 family.

Results and Discussion

Structures of Ca^{2+}-Free and Ca^{2+}-Bound S100A6: The Ca^{2+} Sensor Mechanism

Two different crystal forms of *E. coli*-expressed human S100A6 were obtained for both the Ca^{2+}-free and Ca^{2+}-bound states (see Experimental Procedures). Whereas one of the Ca^{2+}-free crystal forms (tetragonal $P4_22_12$) diffracted the X-rays to less than 3 Å resolution, the other (orthorhombic $C222_1$) produced a complete dataset to 1.15 Å resolution. Crystals of this second form were used to determine the structure from the anomalous signal of a seleno-methionine derivative. However, since the presence of a single methionine residue in human S100A6 provided insufficient anomalous signal for the determination of the structure, it became necessary to add a second methionine at position 3 (Cys3Met) by site-directed mutagenesis. Subsequent determination of the structure of wild-type Ca^{2+}-free S100A6 confirmed that the Cys3Met mutation had no noticeable effect on the structure (rms deviation of 0.11 Å between Cα atoms). The tetragonal Ca^{2+}-free form was then determined by molecular replacement and refined independently to 3.5 Å resolution. Because of its lower resolution, this last structure will not be extensively discussed here. It is important to notice, however, that the Cα atoms of the two Ca^{2+}-free crystal forms superimpose with an rms deviation of 0.56 Å, indicating that in spite of the different crystallization temperatures, buffer conditions, and crystal packing, the structures are nearly identical. Monoclinic (C2) and orthorhombic ($P2_12_12$) crystals of Ca^{2+}-bound S100A6 were obtained under identical crystallization conditions (see Experimental Procedures). Both Ca^{2+}-bound structures were determined by molecular replacement and refined to resolutions of 1.44 Å (C2 form) and 1.76 Å ($P2_12_12$ form). The rms deviation between the Cα atoms of the two Ca^{2+}-bound structures is 0.75 Å. In all the structures, regardless of whether or not Ca^{2+} is bound, S100A6 forms dimers. However, only in one of the crystal forms, orthorhombic ($P2_12_12$) Ca^{2+}-bound S100A6, the dimer is contained within the asymmetric unit, whereas in the others, the dimers are formed by crystal symmetry operators. Throughout this work, comparison of the two states of S100A6 is based on the two highest resolution structures (i.e., monoclinic C2 Ca^{2+}-bound and orthorhombic $C222_1$ Cys3Met Ca^{2+}-free.)

Comparison of these structures clearly highlights the conformational changes upon Ca^{2+} binding that characterize S100A6 as a Ca^{2+} sensor. In both the Ca^{2+}-free and Ca^{2+}-bound states, the overall fold of the monomers consists of four helices and three loops. These elements of secondary structure are arranged into two Ca^{2+} binding motifs known as the S100-hand (H I–L I–H II) and the canonical EF-hand (H III–L III–H IV), which comprise Ca^{2+} binding sites 1 and 2, respectively. The two Ca^{2+} binding motifs are connected by the variable linker loop, L II (Figure 1). The regions of the structures that change the least between the Ca^{2+}-free and Ca^{2+}-bound states are helix I and the N-terminal two-thirds of helix IV, which account for most of the hydrophobic interactions that hold the dimers together. The N-terminal S100-hand undergoes fewer changes on Ca^{2+} binding than the canonical C-terminal EF-hand.

Within the N-terminal S100-hand, the most noticeable difference upon Ca^{2+} binding is a displacement of helix II that can be described as two perpendicular translations of ~4.2 Å toward helix I and ~1.8 Å along its own axis in the direction of the Ca^{2+} binding site (Figure 1C). Notice, however, that this movement of helix II does not lead to any significant difference in interhelical angles (Table 1). The displacement of helix II seems to be driven by the strong bidentate coordination of the Ca^{2+} by the side chain carboxylic group of Glu33 located at the beginning of this helix. Upon Ca^{2+} binding, Glu33 moves ~2.7 Å toward the Ca^{2+}, displacing a water molecule present in the Ca^{2+}-free form (Figures 2A and 2C). In addition to Glu33, the pentagonal bipyramidal coordination of the Ca^{2+} in this site is completed by a water molecule and the main chain carbonyls of Ser20, Glu23, Asp25, and Thr28, which add to a total of 14 amino acids between the first and last Ca^{2+} ligands (Figure 2C). In the Ca^{2+}-free state, there are two well-defined water molecules in site 1, displaying temperature factors of 9.3 $Å^2$ and 15.5 $Å^2$. These water molecules compensate for most of the interactions involving the metal ion in the Ca^{2+}-bound state, thus helping to keep the conformation of site 1 largely unchanged after Ca^{2+} binding (Figure 2A).

In contrast, the C-terminal EF-hand undergoes a major conformational change upon Ca^{2+} binding. Superimposition of the N-terminal two-thirds of helix IV from the Ca^{2+}-free and Ca^{2+}-bound structures highlights a dramatic ~86° reorientation of the amphiphilic helix III (Figure 1D). This measure provides a more accurate estimate of the extent of the conformational change than the traditional calculation of the interhelical angles within each individual structure (listed in Table 1). In the Ca^{2+}-free structure, four hydrophobic residues from the inner face of helix III (Ile53, Leu56, Met57, and Leu60) participate in a hydrophobic cluster with residues from helix II (Leu34, Leu37, Ile38, and Leu42), the linker loop II (Ile44, Lys47, and Leu48), and helix IV (Phe76, Ala79, Leu80, Leu82, and Ile83). The majority of these side chains become solvent-exposed upon Ca^{2+} binding and, as suggested by the structures of S100 proteins with bound peptides [8, 9, 26], participate in target binding.

While the coordination of the Ca^{2+} in site 1 is largely mediated by main chain carbonyls (Figure 2C), the Ca^{2+} ligands in site 2 include, in addition to a water molecule and the main chain carbonyl of Glu67, the side chains of Asp61, Asn63, Asp65, and Glu72 (Figure 2D). Glu72, in particular, is equivalent to Glu33 of site 1. Both glutamates form bidentate interactions with the Ca^{2+} and constitute the last ligand in their respective Ca^{2+} binding loops, occupying position number 4 of the C-terminal

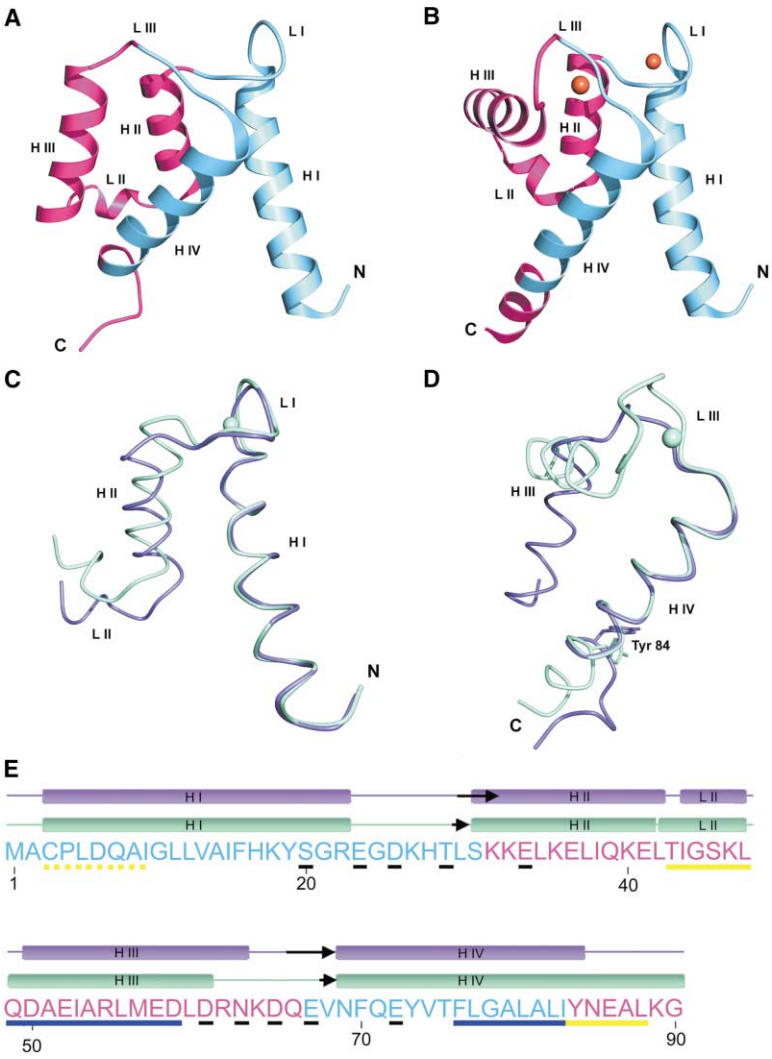

Figure 1. Ribbon Representation of the S100A6 Monomer in the Ca^{2+}-Free and Ca^{2+}-Bound States

After superimposing the structures corresponding to the Ca^{2+}-free and Ca^{2+}-bound states, regions that display the major conformational change (defined as those for which the Cα positions deviate by more than 2.0 Å) are represented in pink (A and B). These include parts of the Ca^{2+} binding loops, helix II, the linker loop II, helix III, and the C-terminal end of helix IV. Notice that helix I and the N-terminal two-thirds of helix IV, which form the intermonomer interface, change less upon Ca^{2+} binding (cyan). In (C) and (D) are shown the superimpositions of the N-terminal S100-hand and C-terminal (canonical) EF-hand in the Ca^{2+}-free (purple) and Ca^{2+}-bound (green) states. Notice how helix II undergoes translations in two perpendicular directions and helix III undergoes a major rotation (~86°) after Ca^{2+} binding. The side chain of Tyr84, the amino acid that marks the starting point for the unwinding of helix IV, is also shown in (D) for the two structures. Using the same color scheme as in (A) and (B), the amino acid sequence of S100A6 is shown in (E) (pink and cyan), illustrating how different regions of the sequence are affected by Ca^{2+} binding. The amino acids implicated in the coordination of the metal ion in the two Ca^{2+} binding loops are underlined (black). Also underlined (blue and yellow) are the regions that, by analogy with the three known structures of S100 protein-peptide complexes, are predicted to participate in target binding in S100A6. The blue lines correspond to the target binding site as observed in the structure of S100B-p53 regulatory peptide [26]; the yellow lines indicate the target binding site according to the structures of S100A10-annexin II [8] and S100A11-annexin I [9] (where the dash and continuous traces indicate the fact that the binding interface in the two annexin complexes includes interactions with the two monomers). See also Figure 4 for a model that combines these two target binding modes into a single and contiguous site. Superimposed on the sequence are representations of the secondary structures of Ca^{2+}-free (purple) and Ca^{2+}-bound (green) S100A6, defined by the main chain hydrogen bonding pattern (α helices and β strands are represented by cylinders and arrows, respectively). Notice that there are differences in the length of helices II, III, IV, the linker loop II, and the β strands connecting the Ca^{2+} loops. The β sheet that connects the two Ca^{2+} binding loops includes three amino acids from each loop in the Ca^{2+}-free state, but only one in the Ca^{2+}-bound state. (Although reports of Ca^{2+}-bound structures of S100 proteins usually refer this to as a β sheet, strictly speaking, the β sheet does not exist in the Ca^{2+}-bound state; i.e., two hydrogen bonds connecting the main chain backbone of two amino acids do not define a β sheet.)

helix of each motif (i.e., helices II and IV). Asp61 and Asn63, which in the Ca^{2+}-free state are part of helix III, move by ~13 Å in order to coordinate the Ca^{2+}. This, in effect, shortens helix III by two amino acids (Figure 1E).

Table 1. Interhelical Angles[1] of S100A6 in the Ca^{2+}-Free/Ca^{2+}-Bound States

	H I	H II	H III	H IV
H I	—	132.2/135.6	−39.5/−107.5	117.6/129.0
H II		—	−144.0/116.5	−46.5/−27.5
H III			—	−157.0/117.3

The definition of helices I to IV in the Ca^{2+}-free and Ca^{2+}-bound states is as in Figure 1.

[1] Interhelical angles (°) were calculated using the program interhlx (Kyoko Yap, University of Toronto).

Thus, it appears that the interactions of Asp61 and Asn63 with the Ca^{2+} constitute a major factor in driving the reorientation of helix III.

Another difference between the two Ca^{2+} states is that the C-terminal helix IV is approximately two turns shorter in the Ca^{2+}-free state. Similar differences in the length of helix IV, depending on whether or not Ca^{2+} is bound, have been previously observed for S100B and S100A6 [25, 27, 31]. The unwinding of helix IV in the present crystal structure of Ca^{2+}-free S100A6 begins at Tyr84, whose side chain rotates by ~45° between the two structures (Figure 1D). In the Ca^{2+}-free structure, the aromatic ring of Tyr84 of one monomer is constrained within a hydrophobic cluster formed by the side chains of Leu42, Ile44, Lys47, Ile53, and Leu80 from the same monomer, while its OH is hydrogen bonded to the

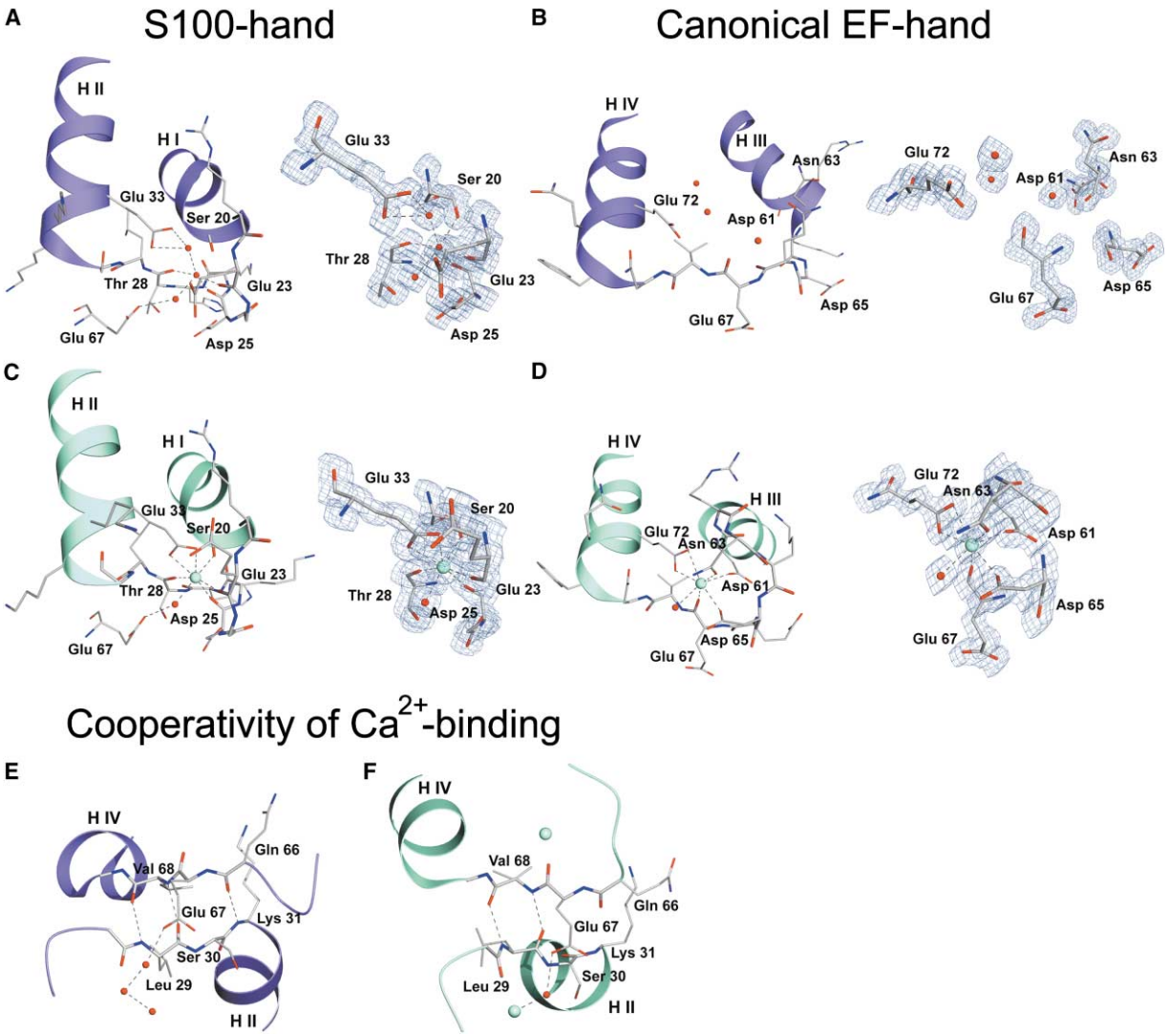

Figure 2. Representation of the S100-Hand and Canonical EF-Hand

The Ca^{2+} binding sites 1 (A and C) and 2 (B and D) are shown in the Ca^{2+}-free (purple) and Ca^{2+}-bound (green) states. Also shown are the 2Fo-Fc electron density maps (contoured at 1.5 σ) around the amino acids that participate in the coordination of the Ca^{2+}. The maps were calculated at 1.15 Å (Ca^{2+}-free) and 1.44 Å (Ca^{2+}-bound) resolution. The coordination of the Ca^{2+} in both sites follows a pentagonal bipyramidal arrangement. In S100A6 (as in most S100 proteins), the S100-hand contains two more amino acids in the Ca^{2+} binding loop than a typical (parvalbumin-like) EF-hand (14 versus 12). Notice that while site 1 undergoes very limited changes upon Ca^{2+} binding, site 2 undergoes a major rearrangement. In the Ca^{2+}-free structure, two water molecules in site 1 seem to account for most of the interactions involving the metal ion in the Ca^{2+}-bound state. With the exception of the bidentate carboxyl group of Glu33 and a water molecule, the coordination of the Ca^{2+} in this site primarily involves main chain carbonyls. In contrast, Ca^{2+} is coordinated in site 2 by the side chains of Asp61, Asn63, Asp65, the bidentate carboxyl group of Glu72, a water molecule, and the main chain carbonyl of Glu67. Notice how the side chain of this last glutamate also coordinates a water molecule in site 1 (A and C). This water molecule then participates in the coordination of the Ca^{2+} in site 1, thus providing a potential link for cooperativity between the two sites. Another view of Glu67, together with a representation of the β sheet that connects the two Ca^{2+} binding sites, is provided in (E) and (F). In the Ca^{2+}-bound structure, the β sheet involves only one amino acid from each site, Leu29 and Val68 (see also Figure 1E).

Oδ1 atom of Asp6 from the second monomer. Such an orientation of the side chain of Tyr84 is responsible for a break in the main chain hydrogen bonding pattern of helix IV. Ca^{2+} binding overcomes the hydrophobic interactions that keep this cluster together, exposing these side chains to the solvent. This appears to trigger the rotation of the side chain of Tyr84 to form new hydrophobic contacts with the side chains of Ile9 and Val13 from the second monomer. The new orientation of the side chain of Tyr84 is consistent with a longer helix IV. Interestingly, a change in the microenvironment of Tyr84 upon Ca^{2+} binding has also been detected by fluorescence studies [32].

It has been suggested that the specificity of interaction with targets may be mediated by the linker loop II, which exhibits the lowest sequence similarity among all

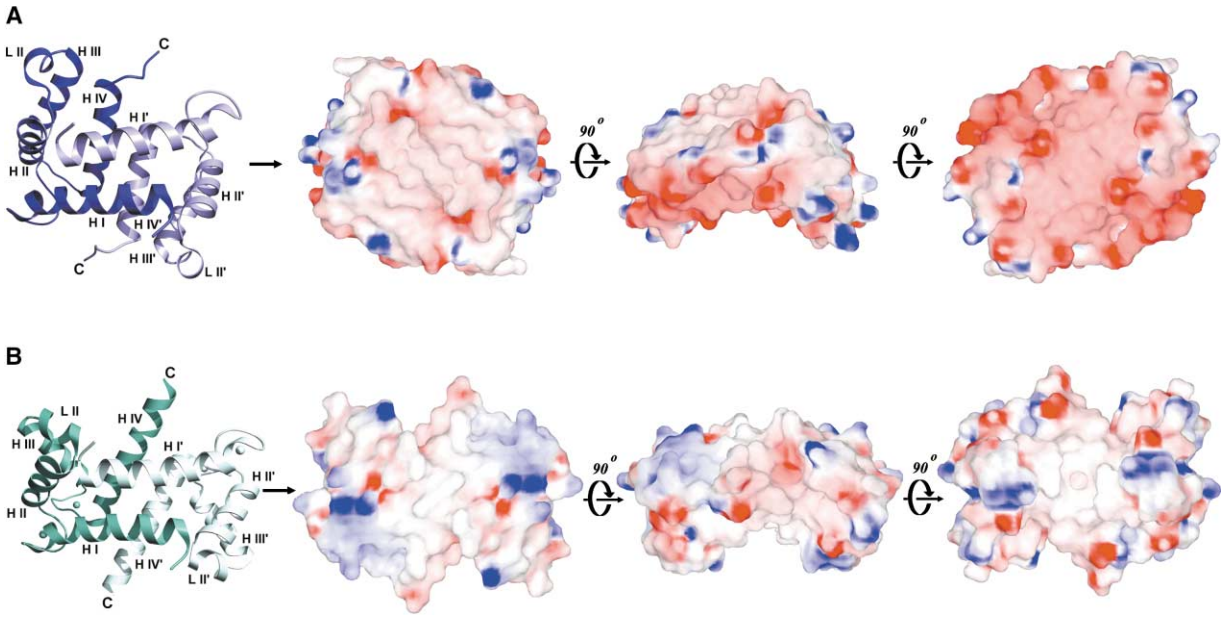

Figure 3. Electrostatic Surface Representation of the S100A6 Dimers in the Ca^{2+}-Free and Ca^{2+}-Bound States

The full-charge electrostatic potential calculation was performed with program GRASP [50]. Red and blue areas indicate negatively and positively charged regions, respectively. Three views of the molecules are shown for each state rotated in increments of 90° (A and B). Notice how the electrostatic charge distribution on one side of the molecule (facing helices I and I′) is less dramatically affected than the opposite side (facing helices IV and IV′) by Ca^{2+} binding. Thus, Ca^{2+}-bound S1006 can be clearly distinguished from its Ca^{2+}-free counterpart as a globally more hydrophobic state. Notice also how Ca^{2+} binding brings about marked changes in the shape of the molecule, creating two symmetrically positioned target binding sites (see also Figure 4). The Ca^{2+}-bound dimer exposes a surface of 9549 Å^2 to the solvent as compared to 9136 Å^2 for the Ca^{2+}-free state.

S100 proteins [5, 33]. In Ca^{2+}-free S100A6, the loop contains a short 1.5 turn helix, which is extended to 2 turns in the Ca^{2+}-bound structure (Figure 1E). The orientation and position of the loop are also different between the two states. In the Ca^{2+}-bound structure, the loop becomes more exposed to the solvent, uncovering the hydrophobic side chains of Leu42, Ile44, and Leu48.

In summary, the major changes upon Ca^{2+} binding to sites 1 and 2 involve helices II and III, respectively, which are connected by the linker loop II. Within the homodimer, helices II and II′, the linker loops II and II′, and helices III and III′ form the most solvent-exposed area of the molecule (Figure 3). Thus, the Ca^{2+} sensor mechanism of S100A6 can be pictured as the Ca^{2+}-dependent opening/closing of two oppositely oriented "arms" (H II–L II–H III and H II′–L II′–H III′) connected to a central, relatively fixed "core" region (H I–H IV–H I′–H IV′). In addition, the last approximately two turns of helices IV from each monomer are part of the external Ca^{2+}-switchable area. We speculate that other members of the S100 family share this mechanism. Although the solution structures of Ca^{2+}-free and Ca^{2+}-bound rat S100B [24, 28] support similar conclusions, they differ markedly from the two S100A6 states reported here. For instance, there is an ~20° difference between the orientation of helix III in the structure of Ca^{2+}-free S100A6 reported here and that of Ca^{2+}-free S100B [28]. However, our results are in more obvious disagreement with previous structures of rabbit S100A6, which display only modest differences between the Ca^{2+}-free and the Ca^{2+}-bound states, thus failing to reveal the existence of Ca^{2+}-induced conformational switch [23, 29, 31].

Cooperativity of Ca^{2+} Binding

EF-hand Ca^{2+} binding loops generally occur in pairs, allowing for positive free energy coupling (cooperativity) between Ca^{2+} binding sites. This aspect of Ca^{2+} binding has been studied better in the case of calmodulin [34], troponin C [35], and calbindin D_{9k} [36]. As compared with calmodulin or troponin C, which have nearly symmetric Ca^{2+} binding loops, cooperativity may involve a different mechanism in S100 proteins, where the Ca^{2+} binding loops are markedly different. The determination in this study of atomic resolution structures of both the Ca^{2+}-free and Ca^{2+}-bound states provides a unique opportunity to identify structural elements that may be relevant to cooperativity (Figures 2E and 2F).

In the Ca^{2+}-free state, a short two-stranded antiparallel β sheet between amino acids Leu29-Lys31 and Gln66-Val68 connects the Ca^{2+} binding sites 1 and 2. Interestingly, in the Ca^{2+}-free state, the hydrogen bonding pattern is consistent with the last two amino acids of the β strand from site 1 (Ser30 and Lys31) being simultaneously assigned as the first two amino acids of helix II (Figure 1E). In the Ca^{2+}-bound structure, the β sheet is shortened to just two hydrogen bonds between the carbonyls and amides of Leu29 from site 1 and Val68 from site 2 (Figures 2E and 2F). Thus, the structures seem to suggest that Ca^{2+} binding to one of the sites

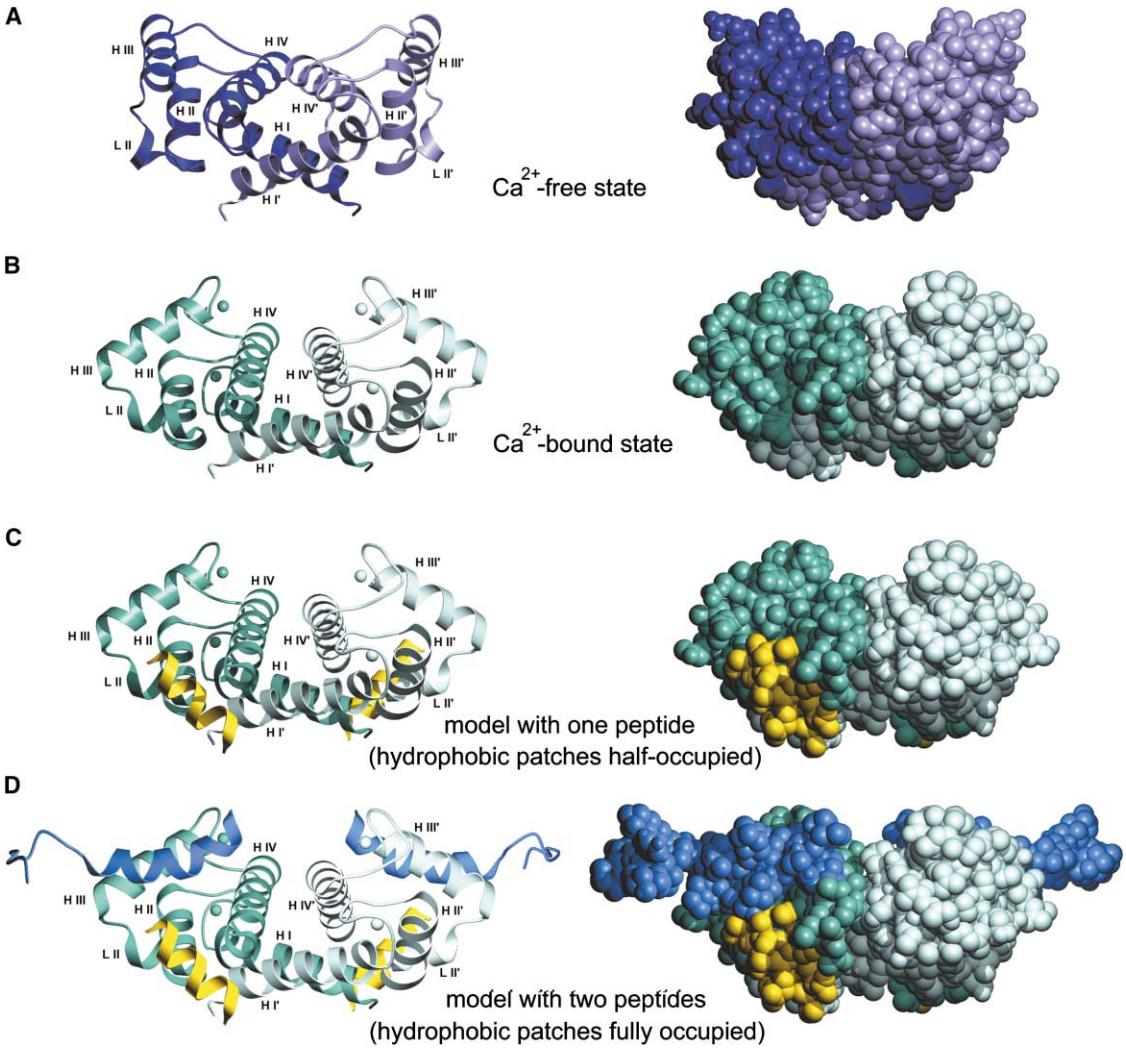

Figure 4. Model of Target Binding

Ribbon and all-atom surface representations are shown side-by-side for the S100A6 dimers in Ca^{2+}-free (A), Ca^{2+}-bound (B), Ca^{2+}-bound with one target peptide modeled as in the structures of S100A10-annexin II [8] and S100A11-annexin I [9] (C), and Ca^{2+}-bound with two target peptides bound to the hydrophobic patches (D), where the second peptide is modeled from the superimposition of the S100B-p53 structure [26] on that of Ca^{2+}-bound S100A6. The color scheme is as in previous figures (Ca^{2+}-free: purple and Ca^{2+}-bound: green, where the two different intensities of the colors represent the two separate monomers that conform the S100A6 homodimer). The annexin II and p53 peptides are shown in yellow and blue, respectively. Two symmetric hydrophobic patches become exposed upon Ca^{2+} binding. Because the annexin [8, 9] and p53 [26] peptides bind to different parts of these patches, a number of hydrophobic amino acids remain exposed in each case. It is possible that binding of full-length targets incorporates elements from both modes of binding, effectively integrating the two target binding sites into a single extended site (as shown in [D]).

weakens the β sheet that connects the two sites. An additional link between the two Ca^{2+} sites is provided by the side chain of Glu67 from site 2, which in both the Ca^{2+}-free and Ca^{2+}-bound states helps coordinate a water molecule in site 1 (Figure 2). In the Ca^{2+}-bound structure, this water molecule is one of the ligands of the Ca^{2+}. Hence, Glu67 may signal the binding of Ca^{2+} from one site to the other.

Although most of the biochemical data (reviewed in [37]) are consistent with a two-step Ca^{2+} binding model, it remains unclear which of the two sites binds Ca^{2+} first. Moreover, the structures alone cannot provide an answer to this question. If we assume, for example, that Ca^{2+} binds first to the higher affinity site 2, this will probably result in a concomitant movement of Glu67 and shortening of the β sheet between the two Ca^{2+} sites, which may, respectively, rearrange the water structure and increase the flexibility of site 1, thus favoring Ca^{2+} binding to this site.

The Ca^{2+}-Free and Ca^{2+}-Bound Dimers: Implications for Target Binding

The biologically functional unit for most S100 proteins is a dimer [5]. Although the hydrophobic interactions that hold the S100A6 dimer together are not significantly altered by Ca^{2+} binding, the intermonomer contact sur-

Table 2. Data Collection, Refinement, and Model Quality Statistics

	Ca^{2+}-Free (Cys3Met)	CA^{2+}-Free Wild-Type	Ca^{2+}-Bound Form 1	Ca^{2+}-Bound Form 2
Data collection				
Space group	$C222_1$	$C222_1$	C2	$P2_12_12$
Unit cell parameters				
a, b, c (Å)	37.3, 48.1, 83.5	37.4, 48.0, 83.0	45.2, 39.2, 48.1	56.6, 58.4, 51.0
α, β, γ (°)	90, 90, 90	90, 90, 90	90, 110.4, 90	90, 90, 90
Resolution range (Å)	30–1.15	30–1.9	15–1.44	19.2–1.75
Completeness (%)	88.2	99.8	99.8	97.4
Number of observations total/unique	399,427/25,856	40,635/6,136	53,548/14,330	74,706/16,853
Redundancy	14.8	6.6	3.7	4.4
χ^2	1.333	1.08	1.04	1.217
Rmerge(%)[1]	6.5	6.7	5	6.1
R^2merge(%)[2]	6.1	6.9	7.2	6.2
Average I/sigma	25.5	13.3	22.2	18.2
Refinement and model quality				
Resolution range (Å)	20.0–1.15	30.0–1.9	15.0–1.44	19.2–1.76
Completeness (%)	95.2	99.8	99.8	97.4
σ-cutoff	none	none	none	none
Rfactor (%; all reflections)[3]	18.6	17.6	21.2	18.5
Free Rfactor (%)[4]	22	18.2	23.1	19.9
Rms deviations				
Bond distance (Å)	0.015	0.006	0.004	0.008
Bond angles (°)	2.5	1.28	1.04	1.34
Dihedral angles (°)	20.4	19.84	18.21	18.79
Improper angles (°)	2.07	0.76	0.71	0.79
Coordinate error (Å) from				
Luzzati plot	0.16	0.22	0.2	0.18
Sigma	0.09	0.21	0.12	0.11
Average B factors				
Protein atoms	14	18.5	17.8	19.27
Water molecules	30	27.5	29.5	30.14
Ramachandran				
Most favored regions (%)	96.1	96.3	93.9	96.9
Additionally allowed regions (%)	3.9	3.7	6.1	3.1
Generously allowed regions (%)	0	0	0	0
Disallowed regions (%)	0	0	0	0

[1] Rmerge $= \Sigma|I - \langle I\rangle|/\Sigma I$; I is the intensity of an individual measurement and $\langle I\rangle$ its mean value.
[2] R^2merge $= \Sigma(I - \langle I\rangle)^2/\Sigma I^2$
[3] Rfactor $= \Sigma|Fo - Fc|/\Sigma|Fo|$; Fo and Fc are observed and calculated structure factors, respectively.
[4] Free Rfactor: same as Rfactor but calculated for a subset of the reflections (5%), which were omitted during the refinement and used to monitor its convergence.

faces (calculated with the CCP4 program AREAIMOL [38]) differ, being 3018 Å^2 and 2795 Å^2 for Ca^{2+}-free and Ca^{2+}-bound S100A6, respectively. Such a difference, amounting to ~8% of the total interface in the Ca^{2+}-bound state, implies a lower stability of the Ca^{2+}-bound dimer. Lower stability of the dimer in the Ca^{2+}-bound state may also result from the uncovering of the hydrophobic patches. In addition, marked differences due to Ca^{2+} binding are observed in the overall shape and size of the dimers (Figure 3), with the Ca^{2+}-free state being more compact (40 × 29 × 43 Å^3) than the Ca^{2+}-bound state (42 × 31 × 51 Å^3). The total surface exposed to the solvent is smaller in the Ca^{2+}-free (9136 Å^2) than in Ca^{2+}-bound (9549 Å^2) states. The two states are also distinguished by marked differences in their electrostatic surface charge distributions (Figure 3). As indicated by previous studies [25, 39–41], the crystal structures show that the solvent-contacting interface of the Ca^{2+}-bound dimer is less charged and, in some regions, more hydrophobic than that of the Ca^{2+}-free form. These differences are especially pronounced on the helices IV and IV′ face of the dimers (Figure 3).

Differences between the Ca^{2+}-free and Ca^{2+}-bound dimers are central to understanding the mechanism of target recognition. Three structures of S100 proteins bound to target peptides are currently available [8, 9, 26]. The crystal structures of S100A10 in complex with an annexin II peptide [8] and that of S100A11 complexed with a peptide from annexin I [9] are quite similar (rms deviation of 0.87 Å). Such a level of resemblance is remarkable since there is no sequence similarity between the two annexin peptides, and S100A11 binds Ca^{2+} whereas S100A10 does not. In both structures, two annexin peptides per S100 dimer bind to symmetrically positioned sites defined by the C-terminal end of helix IV and the linker loop II of one monomer, and the N-terminal end of helix I′ of the second monomer (Figures 1E and 4C). However, in a separate study [26], binding of a p53 regulatory peptide to S100B takes place through a different site, defined by helices III and IV of the same monomer, and in a nearly perpendicular orientation to that of the annexin peptides. In an attempt to identify which of these two modes of binding may best account for the structural differences observed upon Ca^{2+} binding to S100A6, the structures of the complexes were superimposed on those of Ca^{2+}-free and

Table 3. Multiple Anomalous Dispersion (MAD) Phasing Statistics

Wavelength (Å)	λ_1 = 1.02046	λ_2 = 0.97997	λ_3 = 0.94286
Resolution range (Å)	100–1.6	100–1.6	100–1.6
Completeness (%)	88.4	94	96.6
Number of observations (total/unique)	101,216/9,038	112,088/9,572	136,391/9,857
Redundancy	11.2	11.7	13.8
χ^2	1.082	1.09	1.097
Rmerge(%)[1]/R[2]merge(%)[2]	4.2/4.6	5.9/5.3	4.9/5.0
Number of heavy atom sites	2	2	2
Phasing power[3] (Iso/Ano) Centric	na/na	0.7/na	1.5/na
Acentric	na/1.2	1.0/2.9	2.1/3.2
Rcullis[4] (Iso/Ano) Centric	na/na	0.9/na	0.6/na
Acentric	na/0.94	0.87/0.54	0.51/0.52

[1] Rmerge = $\Sigma|I - \langle I\rangle|/\Sigma I$; I is the intensity of an individual measurement and $\langle I\rangle$ its mean value.
[2] R[2]merge = $\Sigma(I - \langle I\rangle)^2/\Sigma I^2$
[3] Phasing power = rmsd ($|F_H|/E$); F_H is the heavy atom structure factor amplitude and E is the residual lack of closure.
[4] Rcullis = $||F_{PH} - F_P| - F_H|/|F_{PH} - F_P|$; F_P, F_H, and F_{PH} are the protein, heavy atom, and derivative structure factors, respectively.
na = not available.

Ca^{2+}-bound S100A6 (Figure 4). The interface involved in contacts with the peptides in either one of the complexes is inaccessible in Ca^{2+}-free S100A6 (Figure 4A). On the other hand, no significant clash occurs when the complexes are superimposed onto Ca^{2+}-bound S100A6 (Figures 4C and 4D), further supporting the idea that target binding by S100 proteins involves a Ca^{2+}-dependent sensor mechanism. One way to reconcile the fact that the p53 and annexin peptides bind to different areas of the same hydrophobic patch is to assume that the two modes of binding complement each other and coexist upon binding of a full-length target (rather than a peptide). Such a model (Figure 4) would help one to understand two potential concerns about the structure of the S100B-p53 complex. First, it has been proposed that each of the two target binding sites of S100 proteins, which function both as homodimers and heterodimers, may involve simultaneous contacts with residues from both monomers [5]. Although this holds true for the two annexin complexes [8, 9], contacts with the p53 peptide involve only one monomer of the S100B dimer [26]. Second, the annexin complexes, but not the p53 complex, account for extensive interactions with both the linker loop II and the C terminus of helix IV, the two most variable regions in S100 proteins, which have long been predicted to participate in specific target binding [5, 37].

Biological Implications

Considerable interest is being devoted to the study of S100 proteins because of their purported association with a number of human diseases and their importance for the clinical diagnosis of cancer. S100A6, in particular, is overexpressed in certain breast cancer cell lines. The high-resolution crystal structures of Ca^{2+}-free and Ca^{2+}-bound S100A6 reported here should help resolve an ongoing debate about whether or not S100 proteins function as Ca^{2+} sensors. This study provides conclusive evidence for a major conformational change in S100A6 upon Ca^{2+} binding, which includes an $\sim$86° reorientation of helix III in addition to changes in the structure and positioning of helix II, the linker loop II, and the C-terminal end of helix IV. By exposing two symmetrically positioned hydrophobic patches, these changes appear to be critical to the way S100 proteins interact with their effector molecules. Complexes of S100B with a p53 peptide [26] and S100A10 and S100A11 with annexin II and annexin I peptides [8, 9] leave important, albeit different, fractions of the hydrophobic patches exposed to the solvent. Based on the assumption that the entirety of the hydrophobic patches should interact with the biological target, we have advanced here a target binding model that combines elements from the modes of binding of the p53 and annexins peptides. We propose that binding of full-length targets may potentially integrate these two modes of binding into one unique target binding interface. Also compatible with this model would be the idea that certain S100 molecules could bind two different targets either sequentially (as Ca^{2+} increases) or simultaneously. Validation of this model will have to await the determination of the structure of a complex of a S100 protein with its intact molecular effector.

A detailed comparison of the structures of Ca^{2+}-free and Ca^{2+}-bound human S100A6 with equivalent structures of rabbit S100A6 [23, 29, 31] and rat S100B [24, 28] exposes marked differences of the structures in both states. Even though the existence of a Ca^{2+} sensor mechanism has been previously visualized in rat S100B [24, 28], the details of such a mechanism are unlike those reported here for human S100A6. Among the three reported solution structures of S100 proteins in the Ca^{2+}-free state, it is the more thoroughly refined rabbit S100A6 [31] that more closely resembles the structure of human S100A6 described here. We predict that expressed doubts concerning the existence of a Ca^{2+} sensor mechanism in S100 proteins [23] will be removed once a similar level of refinement is attained for the solution structure of Ca^{2+}-bound rabbit S100A6. Moreover, given the striking similarity among the various Ca^{2+}-bound structures of S100 proteins determined to high resolution by X-ray crystallography [7, 19–22], including that of the monomeric Ca^{2+}-buffering protein calbindin D_{9k} [10], the structural variations in the S100 family of calcium binding proteins are likely to be rather limited. Differences in sequence localized within the target binding regions, rather than global structural differences, are more likely to account for the vast diversity of functions and targets observed within this family.

Two routes of communication between the Ca^{2+} binding sites 1 and 2 can be recognized from the high-resolution structures of S100A6 reported here. One route observed in all the structures, independent of whether or not Ca^{2+} is bound, involves the coordination of a water molecule in site 1 by the side chain of Glu67 from site 2. In the Ca^{2+}-bound structures of S100A6, this water molecule coordinates the Ca^{2+} in site 1. An identical link is observed in all the crystal structures of S100 proteins that bind two Ca^{2+} ions per monomer (calbindin D_{9k} [10], S100B [22], S100A11-annexin I peptide [9], and S100A12 [21]), but is absent in the structure of S100A8 [20], which has a divergent loop I where Ca^{2+} is coordinated by five ligands only (instead of seven in S100A6). Thus, Glu67 (or its equivalent in other S100 proteins) may effectively "signal" the binding of Ca^{2+} from one loop to the other. A second route of communication is provided by the two-stranded β sheet that links the two Ca^{2+} binding sites. In Ca^{2+}-free S100A6, the β sheet involves hydrogen bonding contacts between three residues from each of the Ca^{2+} binding sites. However, in all the Ca^{2+}-bound structures listed above (including that of S100A8) [9, 10, 20–22], the β sheet is shorter, consisting of just two hydrogen bonds between the carbonyls and amides of one amino acid from each Ca^{2+} binding site. It is possible that binding of Ca^{2+} to one of the sites, more likely site 2 which has a higher affinity for Ca^{2+}, both weakens the β sheet and alters the water structure of the other site through the Glu67 connection, thus favoring Ca^{2+} binding to the remaining site.

Experimental Procedures

Crystallization

S100A6 was expressed and purified as described by Kordowska et al. [41]. Two crystal forms of Ca^{2+}-bound and two crystal forms of Ca^{2+}-free S100A6 were obtained using the hanging drop vapor diffusion method. Prior to crystallization, the protein was dialyzed against 5 mM sodium cacodylate (pH 6.5), 2.5 mM β-mercaptoethanol, 4 mM L-cysteine, and either 2 mM EGTA (for the crystallization of the Ca^{2+}-free form) or 6 mM $CaCl_2$ (for the crystallization of the Ca^{2+}-bound form). A typical hanging drop experiment contained 2 μl of the protein solution at 20 mg/ml and 2 μl of the reservoir solution. The drops were then stabilized against 0.5 ml of the reservoir solution. The two crystal forms of Ca^{2+}-bound S100A6 (belonging to space groups C2 and $P2_12_12$) were obtained at 20°C and under identical reservoir conditions: 20% polyethylene glycol 5000 monomethyl ether, 30 mM Tris-HCl (pH 7.8), and 8% glycerol. Crystals of wild-type and Cys3Met Ca^{2+}-free S100A6, belonging to space group $C222_1$ and diffracting the X-rays to atomic resolution, were obtained at 20°C from a reservoir solution containing 28% polyethylene glycol 1500, 30 mM sodium cacodylate (pH 7.0), and 6% glycerol. The same conditions were also used for the crystallization of a seleno-methionine (Se-Met) derivative of Cys3Met S100A6 used to solve the structure of Ca^{2+}-free S100A6 (see below). Another Ca^{2+}-free crystal form (tetragonal, space group $P4_22_12$) was obtained at 4°C from 42% polyethylene glycol 400 and 20 mM imidazole (pH 6.8). Crystals of this form diffracted the X-rays to ~3.5 Å resolution only (using our in-house X-ray source).

Data Collection, Structure Determination, and Refinement

A dataset to 1.44 Å resolution was collected at IMCA-CAT beamline 17-ID (APS, Argonne, IL) from a Ca^{2+}-bound crystal of the C2 form (Table 2). A separate dataset was collected to 1.76 Å resolution from a crystal of the $P2_12_12$ form at BioCARS beamline 14-BM-D (APS, Argonne, IL). All the diffraction data were collected at 100 K and were indexed and scaled with programs DENZO and SCALEPACK [42]. The two Ca^{2+}-bound structures were determined by molecular replacement with program AMoRe [43] and using the crystal structure of S100A7 [7] as a search model. Refinement and model building were done with programs wARP-Refmac [44] and O [45] (Table 2).

Datasets from the two crystal forms of Ca^{2+}-free S100A6 were initially collected using our in-house equipment (Rigaku RU-H3RH B X-ray generator, mar345 Imaging Plate detector, Oxford Cryostream low temperature system, and Charles Supper Double Mirror X-ray Focusing System). The structure was solved from the multiple anomalous dispersion (MAD) signal obtained from a seleno-methionine derivative (Table 3). Our first attempt, however, to solve the structure from the MAD signal resulting from the single methionine residue present in wild-type S100A6 (Met57) did not produce an interpretable electron density map. In order to enhance the anomalous signal, an additional methionine residue was introduced by site-directed mutagenesis at position number 3 (Cys3Met). The sulfur atoms of the two methionines in the mutated protein were then substituted with selenium by growing the cells in minimal media supplemented with seleno-methionine. Crystals of this derivative were obtained under identical conditions to those of wild-type S100A6 in space group $C222_1$. A three-wavelength MAD experiment was collected at the BioCARS beamline 14-BM-D (APS, Argonne). The positions of the two selenium atoms in the asymmetric unit of the crystals were located with program SnB [46] and refined with program SHARP [47], resulting in a first set of phases that were further refined by solvent flipping with program SOLOMON [48]. The structure was built and refined automatically with programs wARP-Refmac [44], using a dataset to 1.15 Å resolution collected at BioCARS beamline 14-BM-C (APS, Argonne) from the same crystal that produced the three-wavelength MAD data. The quality of the structures reported here was validated with program PROCHECK [49]. Table 2 summarizes the data collection, refinement, and model quality statistics. (Anisotropic refinement of the two highest resolution structures of Ca^{2+}-free and Ca^{2+}-bound S100A6 is currently underway).

Acknowledgments

This study was supported by NIH grant R01 AR46524 to R.D., American Heart Association (New England Affiliate) Beginning Grant-in-Aid 9960176T to R.D., March of Dimes grant 5-FY99-774 to R.D., and NIH grant P01 AR41637 to C.-L.A.W. Use of the Advanced Photon Source was supported by the U.S. Department of Energy, Basic Energy Sciences, Office of Science, under contract No. W-31-109-Eng-38. Use of the BioCARS facilities was supported by NIH grant RR07707. Use of the IMCA-CAT facilities was supported by the companies of the Industrial Macromolecular Crystallography Association and the Illinois Institute of Technology. We would like to thank the staff members at BioCARS and IMCA-CAT (APS, Argonne, IL) for assistance during data collection and Henry Paulus and Zenon Grabarek for critical reading of this manuscript.

Received: November 16, 2001
Revised: January 17, 2002
Accepted: January 23, 2002

References

1. Berridge, M.J., Lipp, P., and Bootman, M.D. (2000). The versatility and universality of calcium signalling. Nat. Rev. Mol. Cell. Biol. *1*, 11–21.
2. Kawasaki, H., Nakayama, S., and Kretsinger, R.H. (1998). Classification and evolution of EF-hand proteins. Biometals *11*, 277–295.
3. Lewit-Bentley, A., and Rety, S. (2000). EF-hand calcium-binding proteins. Curr. Opin. Struct. Biol. *10*, 637–643.
4. Skelton, N.J., Kordel, J., Akke, M., Forsen, S., and Chazin, W.J. (1994). Signal transduction versus buffering activity in Ca(2+)-binding proteins. Nat. Struct. Biol. *1*, 239–245.
5. Donato, R. (2001). S100: a multigenic family of calcium-modulated proteins of the EF-hand type with intracellular and extracellular functional roles. Int. J. Biochem. Cell Biol. *33*, 637–668.
6. Schafer, B.W., and Heizmann, C.W. (1996). The S100 family

of EF-hand calcium-binding proteins: functions and pathology. Trends Biochem. Sci. *21*, 134–140.

7. Brodersen, D.E., Etzerodt, M., Madsen, P., Celis, J.E., Thogersen, H.C., Nyborg, J., and Kjeldgaard, M. (1998). EF-hands at atomic resolution: the structure of human psoriasin (S100A7) solved by MAD phasing. Structure *6*, 477–489.
8. Rety, S., Sopkova, J., Renouard, M., Osterloh, D., Gerke, V., Tabaries, S., Russo-Marie, F., and Lewit-Bentley, A. (1999). The crystal structure of a complex of p11 with the annexin II N-terminal peptide. Nat. Struct. Biol. *6*, 89–95.
9. Rety, S., Osterloh, D., Arie, J.P., Tabaries, S., Seeman, J., Russo-Marie, F., Gerke, V., and Lewit-Bentley, A. (2000). Structural basis of the Ca(2+)-dependent association between S100C (S100A11) and its target, the N-terminal part of annexin I. Struct. Fold. Des. *8*, 175–184.
10. Svensson, L.A., Thulin, E., and Forsen, S. (1992). Proline cis-trans isomers in calbindin D9k observed by X-ray crystallography. J. Mol. Biol. *223*, 601–606.
11. Engelkamp, D., Schafer, B.W., Mattei, M.G., Erne, P., and Heizmann, C.W. (1993). Six S100 genes are clustered on human chromosome 1q21: identification of two genes coding for the two previously unreported calcium-binding proteins S100D and S100E. Proc. Natl. Acad. Sci. USA *90*, 6547–6551.
12. Calabretta, B., Kaczmarek, L., Mars, W., Ochoa, D., Gibson, C.W., Hirschhorn, R.R., and Baserga, R. (1985). Cell-cycle-specific genes differentially expressed in human leukemias. Proc. Natl. Acad. Sci. USA *82*, 4463–4467.
13. Calabretta, B., Venturelli, D., Kaczmarek, L., Narni, F., Talpaz, M., Anderson, B., Beran, M., and Baserga, R. (1986). Altered expression of G1-specific genes in human malignant myeloid cells. Proc. Natl. Acad. Sci. USA *83*, 1495–1498.
14. Murphy, L.C., Murphy, L.J., Tsuyuki, D., Duckworth, M.L., and Shiu, R.P. (1988). Cloning and characterization of a cDNA encoding a highly conserved, putative calcium binding protein, identified by an anti-prolactin receptor antiserum. J. Biol. Chem. *263*, 2397–2401.
15. Komatsu, K., Andoh, A., Ishiguro, S., Suzuki, N., Hunai, H., Kobune-Fujiwara, Y., Kameyama, M., Miyoshi, J., Akedo, H., and Nakamura H. (2000). Increased expression of S100A6 (calcyclin), a calcium-binding protein of the S100 family, in human colorectal adenocarcinomas. Clin. Cancer Res. *6*, 172–177.
16. Stulik, J., Osterreicher, J., Koupilova, K., Knizek, J., Bures, J., Jandik, P., Langr, F., Dedic, K., Schafer, B.W., and Heizmann, C.W. (2000). Differential expression of the Ca2+ binding S100A6 protein in normal, preneoplastic and neoplastic colon mucosa. Eur. J. Cancer *36*, 1050–1059.
17. Mani, R.S., McCubbin, W.D., and Kay, C.M. (1992). Calcium-dependent regulation of caldesmon by an 11-kDa smooth muscle calcium-binding protein, caltropin. Biochemistry *31*, 11896–11901.
18. Sudo, T., and Hidaka, H. (1999). Characterization of the calcyclin (S100A6) binding site of annexin XI-A by site-directed mutagenesis. FEBS Lett. *444*, 11–14.
19. Szebenyi, D.M., Obendorf, S.K., and Moffat, K. (1981). Structure of vitamin D-dependent calcium-binding protein from bovine intestine. Nature *294*, 327–332.
20. Ishikawa, K., Nakagawa, A., Tanaka, I., Suzuki, M., and Nishihira, J. (2000). The structure of human MRP8, a member of the S100 calcium-binding protein family, by MAD phasing at 1.9 A resolution. Acta Crystallogr. D Biol. Crystallogr. *56*, 559–566.
21. Moroz, O.V., Antson, A.A., Murshudov, G.N., Maitland, N.J., Dodson, G.G., Wilson, K.S., Skibshoj, I., Lukanidin, E.M., and Bronstein, I.B. (2001). The three-dimensional structure of human S100A12. Acta Crystallogr. D Biol. Crystallogr. *57*, 20–29.
22. Matsumura, H., Shiba, T., Inoue, T., Harada, S., and Kai, Y. (1998). A novel mode of target recognition suggested by the 2.0 A structure of holo S100B from bovine brain. Structure *6*, 233–241.
23. Sastry, M., Ketchem, R.R., Crescenzi, O., Weber, C., Lubienski, M.J., Hidaka, H., and Chazin, W.J. (1998). The three-dimensional structure of Ca(2+)-bound calcyclin: implications for Ca(2+)-signal transduction by S100 proteins. Structure *6*, 223–231.
24. Drohat, A.C., Baldisseri, D.M., Rustandi, R.R., and Weber, D.J. (1998). Solution structure of calcium-bound rat S100B(betabeta) as determined by nuclear magnetic resonance spectroscopy. Biochemistry *37*, 2729–2740.
25. Smith, S.P., and Shaw, G.S. (1998). A novel calcium-sensitive switch revealed by the structure of human S100B in the calcium-bound form. Structure *6*, 211–222.
26. Rustandi, R.R., Baldisseri, D.M., and Weber, D.J. (2000). Structure of the negative regulatory domain of p53 bound to S100B(betabeta). Nat. Struct. Biol. *7*, 570–574.
27. Kilby, P.M., Van Eldik, L.J., and Roberts, G.C. (1996). The solution structure of the bovine S100B protein dimer in the calcium-free state. Structure *4*, 1041–1052.
28. Drohat, A.C., Amburgey, J.C., Abildgaard, F., Starich, M.R., Baldisseri, D., and Weber, D.J. (1996). Solution structure of rat apo-S100B(beta beta) as determined by NMR spectroscopy. Biochemistry *35*, 11577–11588.
29. Potts, B.C., Smith, J., Akke, M., Macke, T.J., Okazaki, K., Hidaka, H., Case, D.A., and Chazin, W.J. (1995). The structure of calcyclin reveals a novel homodimeric fold for S100 Ca(2+)-binding proteins. Nat. Struct. Biol. *2*, 790–796.
30. Groves, P., Finn, B.E., Kuznicki, J., and Forsen, S. (1998). A model for target protein binding to calcium-activated S100 dimers. FEBS Lett. *421*, 175–179.
31. Maler, L., Potts, B.C., and Chazin, W.J. (1999). High resolution solution structure of apo calcyclin and structural variations in the S100 family of calcium-binding proteins. J. Biomol. NMR *13*, 233–247.
32. Pedrocchi, M., Schafer, B.W., Durussel, I., Cox, J.A., and Heizmann, C.W. (1994). Purification and characterization of the recombinant human calcium-binding S100 proteins CAPL and CACY. Biochemistry *33*, 6732–6738.
33. Kligman, D., and Hilt, D.C. (1988). The S100 protein family. Trends Biochem. Sci. *13*, 437–443.
34. Linse, S., Helmersson, A., and Forsen, S. (1991). Calcium binding to calmodulin and its globular domains. J. Biol. Chem. *266*, 8050–8054.
35. Grabarek, Z., Grabarek, J., Leavis, P.C., and Gergely, J. (1983). Cooperative binding to the Ca2+-specific sites of troponin C in regulated actin and actomyosin. J. Biol. Chem. *258*, 14098–14102.
36. Linse, S., Brodin, P., Drakenberg, T., Thulin, E., Sellers, P., Elmden, K., Grundstrom, T., and Forsen, S. (1987). Structure-function relationships in EF-hand Ca2+-binding proteins. Protein engineering and biophysical studies of calbindin D9k. Biochemistry *26*, 6723–6735.
37. Heizmann, C.W., and Cox, J.A. (1998). New perspectives on S100 proteins: a multi-functional Ca(2+)-, Zn(2+)- and Cu(2+)-binding protein family. Biometals *11*, 383–397.
38. CCP4 (Collaborative Computational Project 4) (1994). The CCP4 suite: programs for protein crystallography. Acta Crystallogr. D *50*, 760–763.
39. Filipek, A., and Kuznicki, J. (1990). Calcyclin-like protein from Ehrlich ascites tumour cells. Ca2+ and Zn2+ binding, distribution and target protein. Acta Biochim. Pol. *37*, 99–101.
40. Filipek, A., Heizmann, C.W., and Kuznicki, J. (1990). Calcyclin is a calcium and zinc binding protein. FEBS Lett. *264*, 263–266.
41. Kordowska, J., Stafford, W.F., and Wang, C.L. (1998). Ca2+ and Zn2+ bind to different sites and induce different conformational changes in human calcyclin. Eur. J. Biochem. *253*, 57–66.
42. Otwinowski, Z., and Minor, W. (1997). Processing of X-ray diffraction data collected in oscillation mode. Methods Enzymol. *276*, 307–326.
43. Navaza, J. (1994). AMoRe: an automated package for molecular replacemenet. Acta Crystallogr. A *50*, 157–163.
44. Perrakis, A., Morris, R., and Lamzin, V.S. (1999). Automated protein model building combined with iterative structure refinement. Nat. Struct. Biol. *6*, 458–463.
45. Jones, T.A., Zou, J.Y., Cowan, S.W., and Kjeldgaard (1991). Improved methods for binding protein models in electron density maps and the location of errors in these models. Acta Crystallogr. A *47*, 110–9.
46. Weeks, C.M., and Miller, R. (1999). The design and implementation of SnB v2.0. J. Appl. Crystallogr. *32*, 120–124.
47. de la Fortelle, E., and Bricogne, G. (1997). Maximum-likelihood heavy-atom parameter refinement for multiple isomorphous re-

placement and multiwavelength anomalous diffraction methods. Methods Enzymol. *276*, 472–494.
48. Abrahams, J.P., and Leslie, A.G.W. (1996). Methods used in the structure determination of bovine mitochondrial F1 ATPase. Acta Crystallogr. *D52*, 30–42.
49. Laskowski, R.A., MacArthur, M.W., Moss, D.S., and Thornton, J.M. (1993). PROCHECK: a program to check the stereochemical quality of protein structures. J. Appl. Crystallogr. *26*, 283–291.
50. Nicholls, A., Sharp, K.A., and Honig, B. (1991). Protein folding and association: insights from the interfacial and thermodynamic properties of hydrocarbons. Proteins *11*, 281–296.

Accession Numbers

Coordinates have been deposited with the Protein Data Bank. Entry codes are 1K9K (Ca^{2+}-bound $P2_12_12$ form), 1K96 (Ca^{2+}-bound C2 form), 1K8U (Ca^{2+}-free Cys3Met mutant), and 1K9P (Ca^{2+}-free wild-type).